ISSN 1070-3632, Russian Journal of General Chemistry, 2015, Vol. 85, No. 6, pp. 1496–1505. © Pleiades Publishing, Ltd., 2015.
Original Russian Text © G.N. Gubanova, S.V. Kononova, M. Cristea, D. Timpu, K.A. Romashkova, E.N. Korytkova, T.P. Maslennikova, N.N. Saprikina, 2015, published in Zhurnal Obshchei Khimii, 2015, Vol. 85, No. 6, pp. 1032–1042.

Morphology and Mechanical Properties of Polymer–Inorganic Nanocomposite Containing Triple Chain Fibrous Na–Mg Hydrosilicate

G. N. Gubanova[a], S. V. Kononova[a], M. Cristea[b], D. Timpu[b], K. A. Romashkova[a], E. N. Korytkova[c], T. P. Maslennikova[c], and N. N. Saprikina[a]

[a] *Institute of Macromolecular Compounds, Russian Academy of Sciences, Bol'shoi pr. Vasil'evskogo Ostrova 31, St. Petersburg, 199004 Russia*
e-mail: gubanovagn@yandex.ru

[b] *"Petru Poni" Institute of Macromolecular Chemistry, Romanian Academy, Iasi, Romania*

[c] *Grebenschikov Institute of Silicates Chemistry, Russian Academy of Sciences, St. Petersburg, Russia*

Received December 29, 2014

Abstract—A polymer-inorganic nanocomposite of fibrous Na–Mg triple chain hydrosilicate and polyamidoimide based on 4-chloroformyl-(*N*-*p*-chloroformylphenyl)phthalimide and 4,4'-diaminodiphenyl ether has been developed. Morphology and dynamic mechanical properties of the nanocomposite films have been studied. Anisotropy of mechanical properties of the nanocomposite and the pristine polyamidoimide films has been revealed. Introduction of the fibrous filler disrupts the ordered mesomorphic structure of the polymer matrix; its recovery upon heating above the glass transition temperature is possible.

Keywords: polyamidoimide, nanocomposite, morphology, mechanical properties, fibrous triple chain hydrosilicate

DOI: 10.1134/S1070363215060249

The polymer-inorganic nanocomposites with a set of mechanical, thermophysical, dielectric, and transport properties significantly different from those of the initial polymer belong to a class of relatively new materials. Development of such composite materials is a topical issue in view of their potential applications in modern technologies [1–3] including the membrane ones.

Possibilities of application of various tubular nanoparticles as fillers for production of organic-inorganic composites have been considered in [4–7]. Besides carbon nanotubes, the oxide or hydroxide particles including hydrosilicate nanotubes of the chrysotile (a fibrous modification of serpentinite) type have been recognized as efficient modifiers of polymer matrices. The formation mechanism of such nanotubes has been studied in [8–10]; therein, a procedure of targeted hydrothermal synthesis has been developed to prepare the $(Mg,Ni,Fe)_3Si_2O_5(OH)_4$ nanotubes of various morphology and surface activity.

Introduction of 5–20 wt % of the synthetic nanotubes of magnesium hydrosilicate $Mg_3Si_2O_5(OH)_4$ into the polyimide matrix has resulted in a significant enhancement of the thermal stability and the Young's modulus of the nanocomposite, its strength and elongation at break remaining sufficiently high [11]. The barrier properties of the nanocomposites with respect to water and oxygen have been also improved. It has been found that the materials barrier properties depend on the nanotubes content as well as on their orientation in the polymer matrix and the dispersion state [12].

Mechanical, dielectric, and transport properties of polyimide nanocomposites modified with magnesium hydrosilicate nanotubes, carbon nanofibres, and montmorillonite nanoparticles have been compared in [13, 14]. Efficiency of the nanotubes chemical treatment in order to optimize their interactions with the matrix and to improve the Young's modulus of the composite materials has been demonstrated.

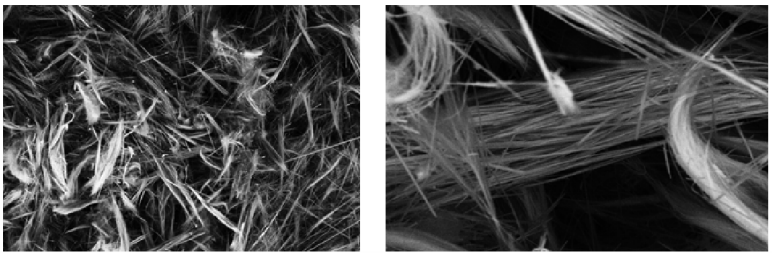

Fig. 1. Scanning electron microscopy images of the Na–Mg triple chain hydrosilicate.

The reports [15, 16] have pioneered in preparation of nanocomposites of polyamidoimides differing in the diamine component structure with the chrysotile type nanotubes of $Mg_3Si_2O_5(OH)_4$. It has been demonstrated that the introduction of up to 10 wt % of the filler improves the mechanical properties (in particular, the Young's modulus) as well as heat and thermal stability of the material [17]. Such materials have been considered promising for the preparation of pervaporation membranes, the optimal transport being attained with 2 wt % of the nanotubes in the composite. The practical interest towards the described material is due to their applications in purification of natural hydrocarbon raw materials from aliphatic alcohols and water [16]. Since any treatment of the filler may change the material transport properties, the comparison of the composite membranes characteristics with these of the starting polyamidoimide seems incorrect. Therefore, the magnesium hydrosilicate nanotubes have been introduced in the polymer matrix without any chemical pre-treatment in the experiments described in [15–17]. It has been demonstrated that the nanotubes form agglomerates, their size and dispersion state being determined by the matrix chemical structure [16, 18]. Structural features of the so formed composites have been studied in view of their importance for the pervaporation behavior of the membranes [17–20]. It has been found that the membrane surface morphology is affected by the content and the distribution pattern of the filler as well as the matrix chemical nature. The modifier particles can be uniformly distributed over the composite membrane volume without being expelled to the surface at relatively low loading of the filler. However, if the nanotubes content is too high (above 5 wt %), part of the nanotubes is pushed out to the surface, the adhesion contact between the matrix and the filler being disrupted; this may result in deterioration of the membrane strength [19].

Besides the tubular hydrosilicates, synthetic fibrous hydrosilicates of the band-chain type are interesting inorganic fillers. A model of the structure of two- and triple chain hydrosilicates based on their X-ray diffraction analysis has been described in [21]. The fibrous hydrosilicates possess valuable engineering properties: they are stable in the corrosive media, highly thermally stable (up to 800°C), and mechanically strong [22]. Synthesis of such nanoparticles is performed under hydrothermal conditions at 250–500°C and pressure above 20 MPa from synthetic mixtures of inorganic compounds as well as from common natural minerals (forsterite, enstatite, talcum, and, serpentinite) or certain industrial tailings [23, 24].

This work aimed to prepare composites based on the polyamidoimide and fibrous nanoparticles of the $Na_2Mg_4Si_6O_{16}(OH)_2$ triple chain hydrosilicate (the hydrosilicate built of three silicon-oxygen chains); such nanoparticles significantly differed from the earlier studied $Mg_3Si_2O_5(OH)_4$ nanotubes. The morphology, thermophysical, and dynamic mechanical properties of the prepared materials have been studied and analyzed accounting for the nanoparticles structure.

Electron microscopy images of the synthesized fibrous nanoparticles of the triple chain hydrosilicate are shown in Fig. 1. As seen, the prepared nanoparticles were formed of the 0.05–0.2 mm long and 10–100 nm thick fibers arranged in bundles. Besides the triple chain hydrosilicate fibers, admixture of thin needle-like nanoparticles (0.2–0.5 mm long and 10–50 nm thick) was observed, assigned to the double chain Na–Mg hydrosilicate (the richterite amphibole).

The structure of the synthesized triple chain hydrosilicate and the presence of the two-row hydrosilicates (amphiboles) [22] admixture were confirmed by the X-ray diffraction pattern of the product (Fig. 2).

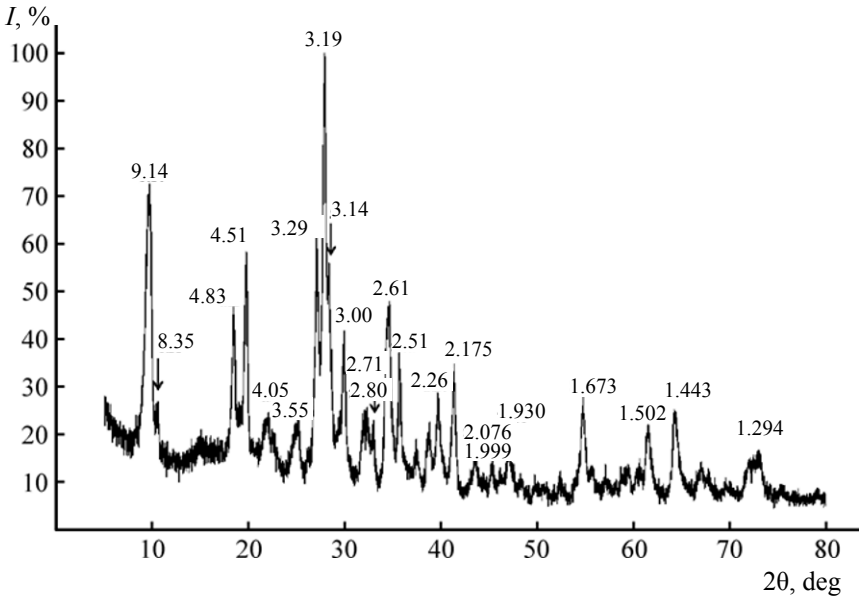

Fig. 2. X-ray diffraction patterns of the prepared fibrous Na–Mg triple chain hydrosilicate. Arrows point at the reflections assigned to the double chain hydrosilicate admixture.

Results of thermogravimetric analysis of the starting polyamidoimide and its composite with the triple chain hydrosilicate at 25–620°C are collected in Table 1. In both cases, three stages of the mass loss were observed: the marginal (<2%) decrease of the mass up to 110°C (elimination of water traces); evaporation of the residual solvent (*N*-methyl-2-pyrrolidone) at 180–300°C, and sharp mass loss above 460°C (the thermal decomposition onset). The observed mass loss and the corresponding temperature ranges were practically the same for the starting polyamidoimide and the composite; hence, incorporation of the fibrous triple chain hydrosilicate in the polyamidoimide matrix neither improved the material thermal stability nor slowed down the solvent release from the film. Those features distinguished the polyamidoimide modification with the triple chain hydrosilicate from the earlier studied modification by magnesium hydrosilicate nanotubes [17].

The earlier studies by means of atomic force microscopy [19, 25] have revealed the presence of distinct oriented domains on the surface of polyamidoimide membranes; this can be due to either the polymer nature or to the film preparation technique. In view of that, physico-mechanical properties of the nonporous polyamidoimide films and the composites were studied in the directions *1* (perpendicular to the squeegee blade motion direction during the films formation) and *2* (along the blade motion direction). The device for the films formation is sketched in Fig. 3.

Dynamic mechanical tests of the starting polyamidoimide and the composite films cut along the directions *1* and *2* were performed over the –150 to 350°C range, below the thermal decomposition onset (Table 1). Fig. 4a presents the test results for the starting polyamidoimide film cut perpendicular to the direction of the squeegee blade motion. The elastic

Table 1. Thermogravimetric analysis data for the films of polyamidoimide and its composite with the triple chain hydrosilicate[a]

Sample	T_1, °C	T_2–T_3, °C	T_4, °C	Adsorbed water, wt %	Residual solvent, wt %	High-temperature residue (600°C), wt %
Polyamidoimide	103	180–290	460	1.8	13.7	45.3
Polyamidoimide–triple chain hydrosilicate	105	178–296	462	2.0	13.7	45.8

[a] T_1, end of water release; T_2–T_3, range of residual solvent release; T_4, thermal decomposition onset.

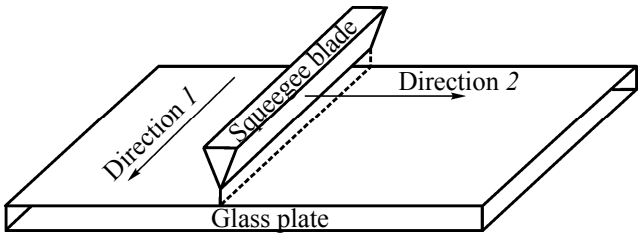

Fig. 3. The device for film preparation (scheme).

modulus of the sample below the glass transition *E*' was 1.65 GPa and decreased upon heating (1 GPa at 150°C and 0.015 GPa at 295°C), noticeably increasing upon further heating. The plots of the loss modulus (*E*") and the loss factor (tan δ) of the same sample as a function of temperature revealed three secondary transitions at –75, 50, and 200°C and the main transition at 291°C. The low-temperature (–75°C) γ transition was assigned to the presence of the frozen adsorbed water; the transition vanished after the sample pre-heating at 150°C. The β relaxation transition observed at 50°C was typical of polyamidoimides and polyimides. That transition temperature generally correlates with the physico-chemical properties (including transport ones) of the polymers [26]. However, there has been no commonly accepted view on the nature of that transition; it has been most often assigned to rotation vibrations of the phenylene and imide groups [27–28].

The transition showing the loss factor maximum at 200°C (the β' transition) and corresponding to the elastic modulus decrease to 0.2 GPa was assigned to elimination of the solvent (*N*-methyl-2-pyrrolidone) in the course of the film heating [17, 19]. The polymer polar groups formed hydrogen bonds with the solvent molecules, those bonds were destroyed upon heating. The solvent release off the polymer material was accompanied by the liberation of the polyamidoimide functional groups and enhancement of the polymer chains mobility; that was reflected in the relaxation transition on the loss factor plot as a function of temperature. Pre-heating of the polyamidoimide film at 200°C favored the intermolecular interactions and formation of the better ordered structure, and the β' transition was observed at the higher temperature as a shoulder at the loss factor curve; after the pre-heating above 200°C that transition was not observed at all. Finally, the high-temperature α transition (291°C) was assigned to devitrification of the most ordered parts of

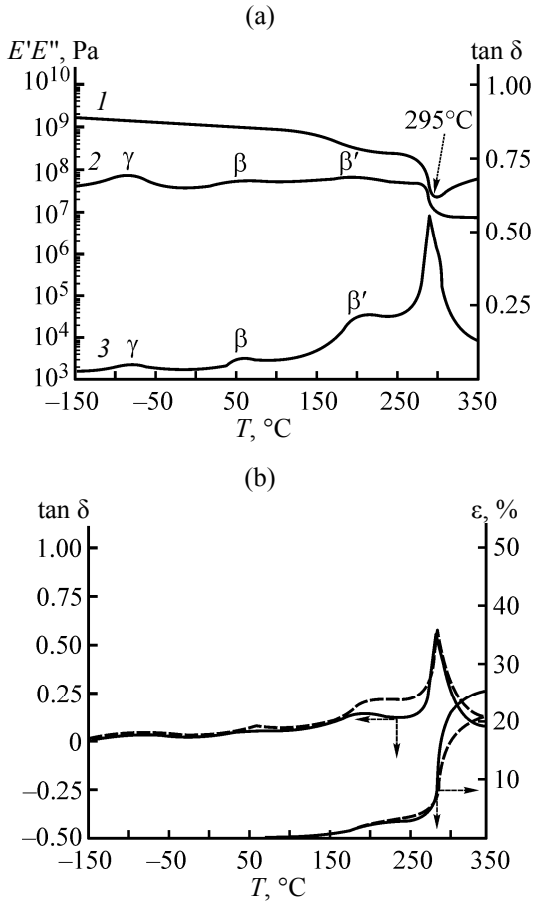

Fig. 4. (a) direction *1*; loss factor tan δ and elongation ε of the (b) polyamidoimide film cut along directions (dashed line) *1* and (solid line) *2*. (*1*) Elastic *E*' and (*2*) loss *E*" modules along with the (*3*) loss factor tan δ of the polyamidoimide film cut along.

the sample. The main α transition was complete at 295°C, the elastic modulus being the lowest at that point (0.015 GPa); the increase in the Young's modulus at further heating will be discussed below.

The plots of elastic and loss modules and loss factor as functions of temperature were qualitatively similar for the film specimens cut along directions *1* and *2*. Selected results of the dynamic mechanical analysis of the films are summarized in Table 2. Note that the elastic modulus of the specimen cut along the direction of the blade motion during the film preparation was significantly higher. The films chemically identical to those used in this work (prepared via the solution casting onto the glass surface followed by the solvent evaporation) have possessed the mesomorphic structure with typically planar orientation of the macromolecules [29, 30]. The formation of the films

Table 2. Temperatures of relaxation transitions and elasticity modulus in the glassy state of the polyamidoimide and its composite with the triple chain hydrosilicate

Sample	E' at –140°C, GPa	T_γ, °C		T_β, $T_{\beta'}$ (°C) (according to tan δ)	T_α, °C			R_α [a]
		according to E''	according to tan δ		according to E'	according to E''	according to tan δ	
Polyamidoimide								
direction *1*	1.65	–82	–80	50; 200	280	285	291	11.0
direction *2*	6.4	–80.5	–76	50; 200	280	284	290	17.3
Polyamidoimide–triple chain hydrosilicate								5.4
direction *1*	1.24	–74	–71	50; 185	285	–	294	
direction *2*	4.4	–77	–74	50; 200	282	–	291	5.6

[a] R_α is a ratio of elasticity modules at the onset (260°C) and at the end (295°C) of the glass transition range.

using the squeegee blade directed likely the predominant orientation of the polymer chains in the casting solution, thus leading to the observed anisotropy of the mechanical properties of the as prepared films (Table 2). That was further confirmed by the anisotropy of positions of the small-angle reflection in the X-ray diffraction patterns (Fig. 5a).

The diffraction patterns of the polyamidoimide samples contained a diffuse halo at 2θ of 19.5° and the small-angle reflections at 2θ of 2.42° (d = 36.4 Å, direction *1*) and 1.67° (d = 53.0 Å, direction *2*). The presence of the small-angle reflections evidenced the mesomorphic state of the polyamidoimide [29, 30].

Anisotropy of mechanical properties of the polyamidoimide films was evident at the elevated temperatures (Fig. 4b); the difference in the loss factor was the most evident at 200–300°C, whereas the relative deformation of the specimens cut along the directions *1* and *2* were different above the glass transition temperature (T > 295°C). Besides the glass transition temperature (T_α), the main α transition can be described by the vitrification temperature range (ΔT_α) and the thermal capacity jump (ΔC_p). The noticeable decrease of the elasticity modulus observed in the dynamic mechanical test over the glass transition range (ΔT_α = 260–295°C) (Fig. 4a) was expressed by the modulus ratio at the start and end points of the vitrification (R_α). That ratio was significantly higher for the direction *2* as compared to the direction *1* (R_α = 17 and 11, respectively, cf. Table 2).

The increase of the elastic modulus upon heating above 295°C (Fig. 4a) measured in the mechanical test

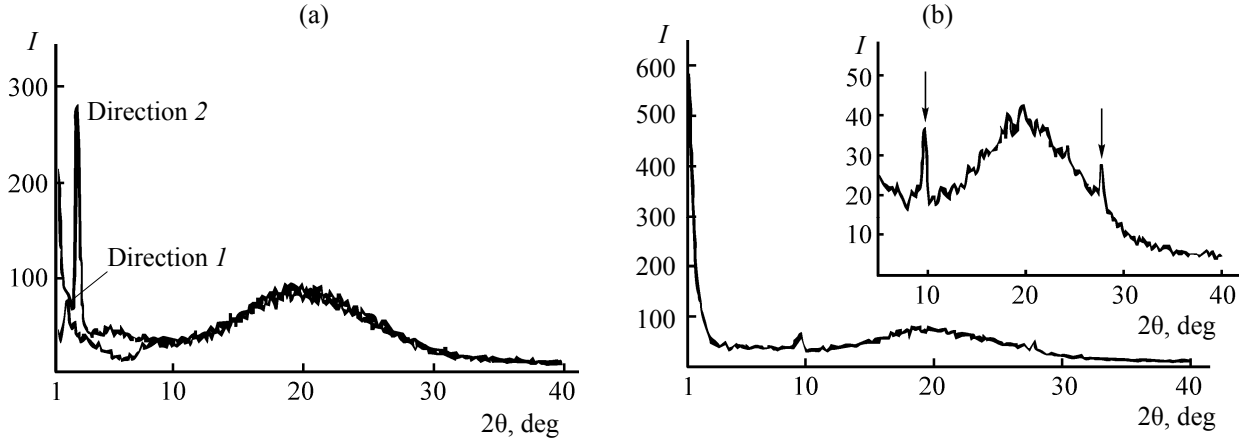

Fig. 5. X-ray diffraction patterns of the (a) polyamidoimide (along directions *1* and *2*) and (b) the composite samples.

was accompanied by noticeable elongation of the polyamidoimide film specimen (Fig. 4b), assigned to the segmental mobility of the macromolecules. Simultaneous increase of the stiffness and the elongation of the specimen could be ascribed to the macromolecules orientation under conditions of the experiment. It has been earlier demonstrated that the increase in the dynamic mechanical modulus of the rigid-chain polyimide films along the uniaxial stretching direction is due to the molecules orientation rather than the increased degree of crystallinity [31]. For the polyimides it has been shown that the domains growth and the macromolecules ordering inside the domain upon the uniaxial stretching are observed at relatively low temperatures (below the polymer T_g) and deformations [32, 33]. Further heating and stretching resulted in orientation of the domains as a whole. Since the polyamidoimide films used in this work existed in the mesomorphic state, the increase of their elastic modulus above the glass transition temperature could be reasonably explained by the orientation of the ordered domains along the stress axis. The influence of temperature on the size and ordering degree of the mesomorphic regions was more pronounced below the α transition temperature, when the specimen elongation was ingorable increased (Fig. 4b).

Let us now analyze the properties of the polyamidoimide nanocomposite with the triple chain hydrosilicate prepared in this work. The filler loading was of 2 wt %; such content has turned optimal in view of the transport properties of the composite with the chemically similar tubular filler [15, 19]. Even though the used loading was not necessarily optimal in the case of the nanocomposites studied in this work, we expected to discover the general features of the fibrous filler influence on the composite properties.

X-ray diffraction pattern of the nanocomposite (Fig. 5b) contained the diffuse amorphous halo at 2θ of 19.5°, typical of the polyamidoimide. The introduction of the such bulky fibrous nanoparticles disordered the macromolecules folding, and the small-angle reflection, observed in the diffraction pattern of the starting polyamidoimide (Fig. 5a), was absent in the case of the nanocomposite film. At the same time, the reflections typical of the triple chain hydrosilicate at 2θ of 9.67° (d = 9.15 Å) and 27.7° (d = 3.22 Å) overlaid the amorphous halo (see inset in Fig. 5b). Note that the introduction of the same amount of the magnesium hydrosilicate nanotubes has not changed the starting polyamidoimide structure, and the reflections typical of the pure filler have not been observed [17]. To summarize, in contrast to the earlier studied tubular hydrosilicate, the triple chain hydrosilicate used in this work as a filler disrupted the mesomorphic structure of the matrix but revealed its own crystalline structure, due likely to the nanoparticles aggregation.

Incorporation of 2 wt % of the triple chain hydrosilicate into the polyamidoimide matrix retained the anisotropy of mechanical properties of the starting polymer film (Table 2). The composite elastic and loss modules as well as loss factor as functions of temperature were qualitatively similar to those of the unfilled polymer (cf. Figs. 4a and 6a). The α transition of the composite film was observed at the temperature practically equal to the starting polyamidoimide glass transition temperature. However, the elastic modules of the composite film in its glassy state in both directions were significantly lower than the corresponding modules of the starting polymer film (Table 2). Hence, the introduction of the fibrous triple chain hydrosilicate did not enhance the composite stiffness as compared to that of the matrix, despite the excellent mechanical properties of the filler. The shift of the γ transition temperature upon the fibrous filler incorporation was also notable; it could be due to the high adsorption ability of those nanoparticles [23, 24].

The increase of elastic modulus and the elongation of the composite above the glass transition temperature (291°C) (Fig. 6b) was less prominent than in the case of the unfilled polyamidoimide. Evidently, the introduction of the fibrous filler decreased the polymer chains flexibility and their orientation became less efficient. The R_α parameter was isotropic in the case of the composite, likely due to the chaotic distribution of the fibrous nanoparticles over the polymer matrix volume.

The elastic modulus of the composite increasing upon heating above the glass transition temperature pointed at recovery of the ordered mesomorphic structure of the polyamidoimide matrix, initially disrupted due to the fibrous filler introduction. The possibility of the reordering due to orientation above the glass transition point has been earlier demonstrated for amorphous aliphatic copolyimides [34, 35]. The molecular origin of the macroscopically similar process in the case of the composite studied in this work needs additional justification.

Decrease in the polyamidoimide elastic modulus after its modification with the triple chain hydrosilicate

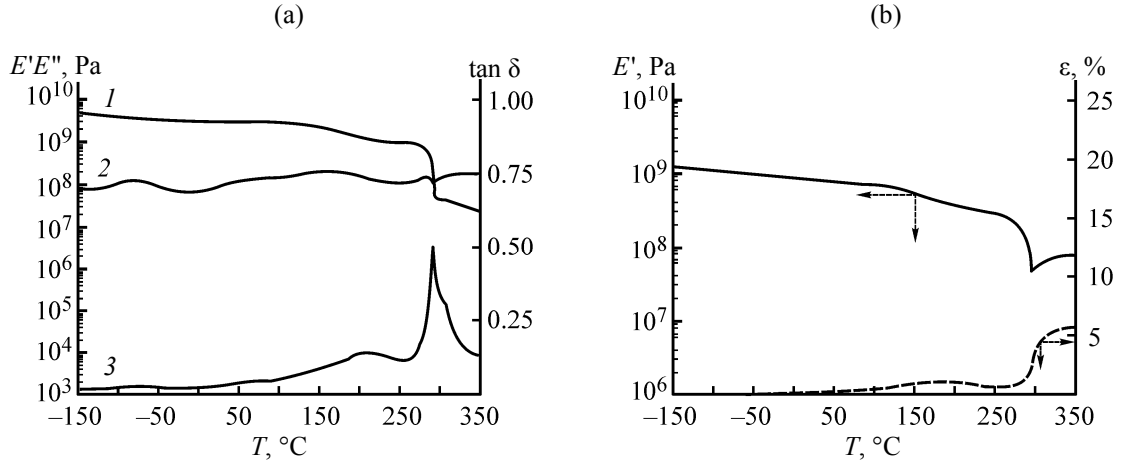

Fig. 6. (*1*) Elastic *E*' and (*2*) loss *E*" modules along with the (*3*) loss factor tan δ of the composite film cut along direction *2* (a); loss factor tan δ (solid line) and elongation ε (dashed line) of the polyamidoimide film cut along direction *2* (b).

could be due to the non-uniform distribution of the fibrous aggregates in the sample volume and to the low degree of the fibres exfoliation within the aggregate. That was confirmed by the scanning electron microscopy data: the images of the composite revealed the presence of the randomly distributed individual fibres of the filler (Fig. 7a) along with the bundled aggregates of the triple chain hydrosilicate fibres (Fig. 7b). The stress is concentrated on such aggregates, thus decreasing the composite strength.

Atomic force microscopy studies of the composite surface revealed neither the fibrous structures nor their fragments (Fig. 7c). Hence, even though the fibrous triple chain hydrosilicate particles were larger than the earlier studied tubular hydrosilicates [15, 16], at the filler content of 2 wt % the fibrous particles were distributed over the polymer film volume without being expelled to the surface. Analysis of AFM images of the cross-sections of the composite film revealed the presence of two phases: the polymer and the inorganic filler (Fig. 7d). The inorganic particles were 20–25 nm thick, coinciding with the filler size according to the scanning electron microscopy studies (Fig. 1). Distance between the fragments of the fibrous structures in the composite was of 2–2.5 μm, larger than that in the initial bundle (Fig. 1). That could be due to the ultrasonic treatment during the nanoparticles dispersing and the efficient interaction between the polar groups at the filler surface and the polymer polar groups. Hence, an optimal choice of the polymer matrix (the one capable of stronger interaction with the filler) could improve the inorganic phase dispersion and the strength of the resulting composite. Another approach towards the composite strength improvement is the dispersing procedure modification, allowing for better orientation of the fibrous nanoparticles in the polymer matrix.

To summarize, in this work we prepared and studied a new polymer-inorganic composite based on polyamidoimide and fibrous Na–Mg hydrosilicate. The results indicate the presence of both the individual nanofibres and their larger aggregates in the composite. Certain mechanical properties of the composite were deteriorated as compared with those of the pure polymer matrix, due to the insufficiently efficient dispersion of the filler. The introduction of the fibrous filler disrupted the ordered mesomorphic structure of the matrix; however, it could be recovered via the orientation processes upon heating above the glass transition temperature. The anisotropy of mechanical properties of the starting and the filled polymer films was demonstrated, assigned to the orientation of the polymer chains along the direction of the films formation.

EXPERIMENTAL

The polyamidoimide (M_w = 65000) was prepared from 4-chloroformyl-(*N*-*p*-chloroformylphenyl)phthalimide and 4,4'-diaminodiphenyl ether (0.01 mol of the each component) via the low-temperature solution polycondensation [36]. The reaction was carried out in *N*-methyl-2-pyrrolidone first at –15°C during 1 h and then at room temperature during 2 h to yield viscous pale-yellow solution.

The fibrous triple chain hydrosilicate $Na_2Mg_4Si_6O_{16}\cdot(OH)_2$ (used as filler) was prepared under hydro-

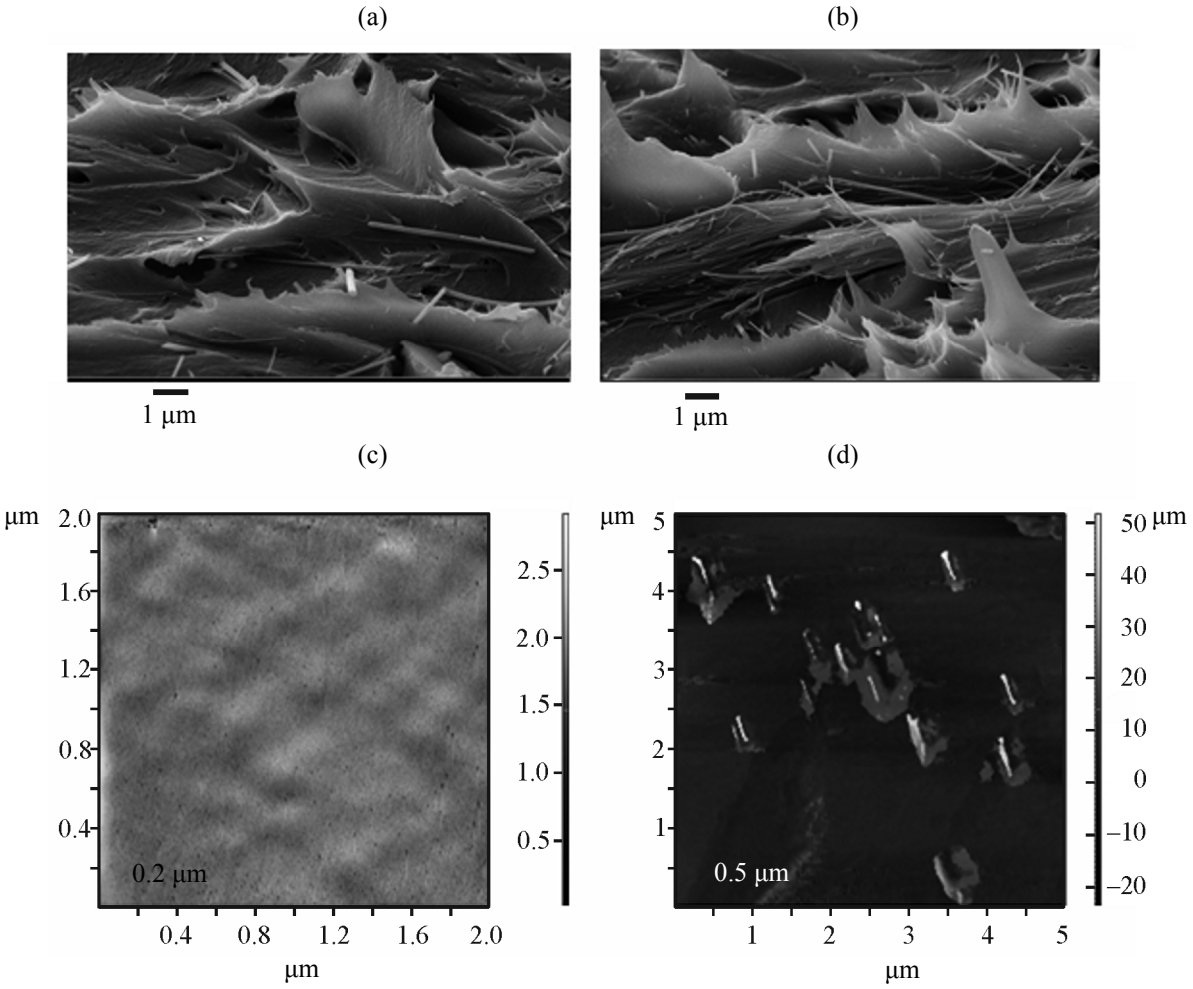

Fig. 7. Visualization of the film of the polyamidoimide composite with the triple chain hydrosilicate: (a, b) the cross-section (SEM) and (d) phase contrast AFM; (c) the surface (topography mode AFM).

thermal conditions at 400°C and 50 MPa (24 h) from a mixture of MgO and SiO_2 in an aqueous solution of NaOH (1 wt % of the alkali). The ratio of magnesium and silicon in the reaction mixture corresponded to the stoichiometry of the hydrosilicate, MgO : SiO_2 = 4 : 6.

The composite was prepared in the *N*-methyl-2-pyrrolidone via ultrasonic treatment (40 kHz) upon mixing the hydrosilicate dispersion in the polyamidoimide solution (in air, at room temperature). The mixing duration (20 h), the polymer concentration (8 wt %), and the filler content (2 wt % with respect to the polymer) were determined according to the earlier reported data [16]. The 35–40 μm thick composite films were prepared via the dispersion casting onto a glass plate followed by the film formation with a squeegee blade and evaporation of the solvent at 150°C.

Dynamic mechanical tests of the films were run using a Perkin Elmer Diamond (USA) device in the elongation mode (1 Hz, heating at 2 deg/min, nitrogen atmosphere); the multi-frequency mode (0.5, 1, 2, 5, and 10 Hz) was used as well. The specimen dimensions were 10 mm × 10 mm × 35–40 μm.

Thermogravimetric analysis was performed using a Q-1500 (Hungary) derivatograph (heating at a rate 10 deg/min, nitrogen atmosphere).

X-ray diffraction studies were run at room temperature using a D8 Advanced BrukerAXS diffractometer (reflection mode, scattering angle 2θ of 1°–40°, scanning step of 0.02°; CuK_α radiation, Ni filter, 36 kV, 36 mA).

Cross-sections of the composite films were observed using a Supra 55VP Zeiss (Germany) scanning electron microscope. The surface electrical conductivity was achieved by contrasting the specimen with gold (15–20 nm, cathodic sputtering, a Quorum 150

device). The secondary electrons mode (SE2) was used in the morphology studies.

Morphology of the surface and low-temperature cross-sections was additionally studied by means of atomic force microscopy using a SPM SOLVER Pro-M device (NT-MDT, Russia). The observations were performed in a semi-contact mode in air using an NSG 10/Au silicon cantilevers with the stiffness coefficient of 11.8 N/m and the curvature of the tip of 6 nm.

ACKNOWLEDGMENTS

This work was financially supported by the Russian Foundation for Basic Research (project 14-08-00887-a).

REFERENCES

1. Paul, D.R. and Robeson, L.M., *Polymer*, 2008, vol. 49, p. 3187. DOI: 10.1016/j.polymer.2008.04.017.
2. Moniruzzaman, M. and Winey, K.I., *Macromolecules,* 2006, vol. 39, p. 5194. DOI: 10.1021/ma060733p.
3. Ober, C.K., Cheng, S.Z.D., Hammond, P.T., Muthukumar, M., Reichmanis, E., Wooley, K.L., and Lodge, T.P., *Macromolecules,* 2009, vol. 42, no. 2, p. 465. DOI: 10.1021/ma802463z.
4. Baker, L.A., Jin, P., Martin, R., *Crit. Rev. Solid State Mater. Sci*., 2005, vol. 30, no. 4, p. 183. DOI: 10.1080/10408430500198169.
5. Rakov, E.G., *Russ. J. Inorg. Chem*., 1999, vol. 44, no. 11, p. 1736.
6. Ivanovskii, A.L., *Russ. Chem. Rev*., 2002, vol. 24, no. 3, p. 175.
7. Rao, C.N.R. and Nath, M., *Dalton Trans*., 2003, p. 1. DOI: 10.1039/B208990B.
8. Chivilikhin, S.A., Popov, I.Yu., Blinova, I.V., Konovalov, A.S., Oblogin, S.I., Tishkin, V.O., Chernov, I.A., Kirillova, S.A., and Gusarov, V.V., *Glass Phys. Chem*., 2007, vol. 33, no. 4, p. 315. DOI: 10.1134/S1087659607040037.
9. Korytkova, E.N., Maslov, A.V., Pivovarova, L.N., Drozdova, I.A., and Gusarov, V.V., *Glass Phys. Chem*., 2004, vol. 30, no. 1, p. 51. DOI: 10.1023/B:GPAC.0000016397.29132.21.
10. Korytkova, E.N., Maslov, A.V., Pivovarova, L.N., Polegotchenkova, Yu.V., Povinich, V.F., and Gusarov, V.V., *Inorg. Mater*., 2005, vol. 41, no. 7, p. 743. DOI: 10.1007/s10789-005-0202-1.
11. Yudin, V.E., Otaigbe, J.U., Gladchenko, S., Olson, B.G., Nazarenko, S., Korytkova, E.N., and Gusarov, V.V., *Polymer*, 2007, vol. 48, p. 1306. DOI: 10.1016/j.polymer.2007.01.012.
12. Wu, Y., Yudin, V., Otaigbe, J., Korytkova, E., Nazarenko, S., *J. Polym. Sci. (B)*, 2013, vol. 51, p. 1184. DOI: 10.1002/polb. 23317.
13. Gofman, I.V., Svetlichnyi, V.M., Yudin, V.E., Dobrodumov, A.V., Didenko, A.L., Abalov, I.V., Korytkova, E.N., Egorov, A.I., and Gusarov, V.V., *Russ. J. Gen. Chem*., 2007, vol. 77, no. 7, p. 1158. DOI: 10.1134/S1070363207070043.
14. Yudin, V.E. and Svetlichnyi, V.M., *Ross. Khim. Zh.*, 2009, vol. 53, no. 4, p. 75.
15. Kononova, S.V., Korytkova, E.N., Romashkova, K.A., Kuznetsov, Yu.P., Gofman, I.V., Svetlichnyi, V.M., and Gusarov, V.V., *Russ. J. Appl. Chem*., 2007, vol. 80, no. 12, p. 2142. DOI: 10.1134/S1070427207120297.
16. Kononova, S.V., Romashkova, K.A., Kruchinina, E.V., Gusarov, V.V., Potokin, I.L., Korytkova, E.N., and Maslennikova, T.P., *Russ. J. Gen. Chem*., 2010, vol. 80, no. 6, p. 1136. DOI: 10.1134/S1070363210060162.
17. Gubanova, G.N., Kononova, S.V., Vylegzhanina, M.E., Sukhanova, T.E., Grigor'ev, A.I., Romashkova, K.A., Svetlichnyi ,V.M., Korytkova, E.N., Cristea, M., Timpu, D., and Harabagiu, V., *Russ. J. Appl. Chem*., 2010, vol. 83, no. 12, p. 2175. DOI: 10.1134/S1070427210120207.
18. Gubanova, G.N., Kononova, S.V., Vylegzhanina, M.E., Korytkova, E.N., Maslennikova, T.P., and Sukhanova, T.E., *Nanotekhnol.: Nauka i Pro–vo*, 2011, no. 5 (14), p. 22.
19. Gubanova, G.N., Kononova, S.V., Bronnikov, S.V., Romashkova, K.A., Sukhanova, T.E., Korytkova, E.N., Timpu, D., Cristea, M., and Harabagiu, V., *J. Macromol. Sci. (B),* 2014, vol. 53, no. 4, p. 555. DOI: 10.1080/00222348.2013.847399.
20. Gubanova, G.N., Vylegzhanina, M.E., Kononova, S.V., Lavrent'ev, V.K., and Sukhanova, T.E., Abstracts of Papers, *XI Mezhdun. konf. "Metodologicheskie aspekty skaniruyushchei zondovoi mikroskopii"* (XI Int. Conf. "Methodological Aspects of Scanning Probe Microscopy"), Minsk, 2014, p. 95.
21. Drits, V.A., Goncharov, Yu.I., Aleksandrova, V.A., Khadzhi, V.E., and Dmitrik, A.L., *Kristallograf*., 1974, vol. 19, no. 6, p. 1186.
22. Grebenshhikov, R.G., Grigor'eva, L.F., and Makarova, T.A., *Vestn. Akad. Nauk SSSR*, 1970, no. 7, p. 63.
23. Korytkova, E.N., Pivovarova, L.N., Grebenshchikov, R.G., and Khadzhi, I.P., *Geokhim*., 1997, no. 7, p. 709.
24. Korytkova, E.N., Sipovskii, D.P., Fedoseev, A.D., and Makarova, T.A., *ZVMO*, 1968, vol. 97, no. 4, p. 500.
25. *Scanning Probe Microscopy – Physical Property Characterization at Nanoscale*, Nalladega, V., Ed., Rijeka: InTech, 2012, p. 81.
26. Huang, S-Y., Hu, C., Lee, K-R., Liaw, D.-J., and Lai, J.-Y., *Eur. Polym. J*., 2006, vol. 42, p. 140. DOI: 10.1016/j.eurpolymj., 2005.06.032.
27. Harris, J.E. and Robeson, L.M., *J. Appl. Polym. Sci*., 1988, vol. 35, p. 1877. DOI: 10.1002/app.1988.070350713.

28. Kochi, M., Chen, C., Yokota, R., Hasegava, M., and Hergenrother, P., *High Perform. Polym*., 2005, vol. 17, p. 335. DOI: 10.1177/ 0954008305055557.
29. Sidorovich, A.V., Svetlichnyi, V.M., Baklagina, Yu.G., Gusinskaya ,V.A., Batrakova, T.V., Romashkova, K.A., and Goikhman, M.Ya., *Vysokomol. Soed. (A)*, 1989, vol. 31, no. 12, p. 2597.
30. Gusinskaya, V.A., Baklagina, Yu.G., Romashkova, K.A., Batrakova, T.V., Kuznetsov, Yu.P., Koton, M.M., Sidorovich, A.V., Mikhailova, N.V., Nasledov, D.M., and Lyubimova, G.N., *Vysokomol. Soed. (A)*, 1988, vol. 30, p. 1316.
31. Smirnova, V.E., Bessonov, M.I., Sklizkova, V.P., and Nekrasova, E.N., *Vysokomol. Soed. (A)*, 1991, vol. 33, no. 11, p. 2445.
32. Lavrent'ev, V.K. and Sidorovich, A.V., *Vysokomol. Soed. (B)*, 1984, vol. 24, no. 1, p. 3.
33. Baklagina, Yu.G., Sidorovich, A.V., Urban, I., Pel'ts-bauer, Z., Gusinskaya, V.A., Romashkova, K.A., and Batrakova, T.V., *Vysokomol. Soed. (B)*, 1989, vol. 31, p. 38.
34. Cristea, M., Ionita, D., Hulubei, C., Timpu, D., and Popovici, D., *Polymer*, 2011, vol. 52, p. 1820. DOI: 10.1016/j.polymer., 2011.02.026.
35. Hasegawa, M., Okuda, K., Horimoto, M., Shindo, Y., Yokota, R., and Kochi, M., *Macromolecules,* 1997, vol. 30(19), p. 5745. DOI: 10.1021/ma970551i.
36. Gusinskaya, V.A., Koton, M.M., Batrakova, T.V., and Romashkova, K.A., *Vysokomol. Soed. (A)*, 1976, vol. 18, no. 12, p. 2681.